

# X-ray Observations of Young Supernova Remnants

Una Hwang

*NASA Goddard Space Flight Center, Greenbelt, MD 20771, and  
University of Maryland, College Park, MD 20742, USA*

## **Abstract.**

This brief review of recent X-ray observations of young supernova remnants highlights results obtained by the Chandra and XMM Newton Observatories since their launch last year. Their impressive capabilities are illustrated by results for spectral imaging, and for spatially resolved spectroscopy that isolates emission from individual ejecta knots and from the forward shock. I also review X-ray dynamical studies of supernova remnants, which should undergo significant advances during this new era.

## **INTRODUCTION**

Young supernova remnants are expected to emit brightly in X-rays, as the forward and reverse shocks in remnants typically heat the ambient gas and ejecta to X-ray emitting temperatures. Moreover, supernova remnants are expected to be rich X-ray emission line sources: the gas ionizes slowly after being suddenly heated behind the shock, so that the populations of certain stable ions can be significantly higher than would be expected at equilibrium for a given electron temperature. The result is correspondingly enhanced line emission from those ions. For remnants whose X-ray emission is dominated by the reverse-shocked ejecta, the line emission will be further enhanced by the high element abundances in the ejecta that result from nuclear processing, both before and during the supernova explosion.

It has been twenty years since early X-ray spectral observations at both moderate and high resolution first verified the rich X-ray emission line spectra of supernova remnants (e.g., Becker et al. [1], Winkler et al. [2]); meanwhile, ever improving X-ray images have revealed their beautiful and complex morphologies (e.g., see Seward [3] and references therein, Aschenbach et al. [4], Levenson et al. [5], Williams et al. [6]). Opportunities for simultaneous imaging and spectroscopy, however, have been limited until relatively recently. The launch of the ASCA satellite in 1993 [7] marked a significant advance, in that 1' optics were coupled with CCD imaging spectrometers of moderate spectral resolution that were capable of isolating certain emission lines and blends. ASCA thus provided the first X-ray spectral images [8,9],

as well as important spatially resolved spectral results for remnants of larger angular size.

In 1999, the launch of Chandra and XMM Newton provided an enormous further advance in that the CCD spectrometers were placed at the focus of far better mirrors—XMM Newton provides a point source image with a roughly  $6''$  core, while Chandra provides a  $0.5''$  angular resolution that is the best ever realized for X-rays. The two missions are complementary, with Chandra's strength being its superior mirrors, and XMM's strength being its higher collecting area, particularly at energies above 5 keV (for example, see the impressive very high energy X-ray image of Cas A taken by XMM [10]). Both missions also include dispersive high resolution spectrometers, with complementary characteristics, that have already provided exciting results for supernova remnants in the Magellanic Clouds (see the review by Canizares [11]). Unfortunately, such observations are difficult for remnants of any significant angular size because of the complicated blending of highly detailed spatial and spectral information.

This review highlights a few of the many results obtained by Chandra and XMM during their first year, with the goal of illustrating the power of simultaneous imaging and spectroscopy with moderate resolution CCD spectrometers. It is restricted to a few illustrative examples of spectral imaging and of detailed spectroscopy of compact regions of thermal X-ray emission from shocked ejecta and ambient gas. Numerous other such examples have been presented at this conference. I conclude by looking forward to the coming of age of X-ray dynamical studies of supernova remnants.

## X-RAY SPECTRAL IMAGING

The capability to image a source in specific spectral features from a single element is particularly important for young supernova remnants whose emission is dominated by their ejecta, as such images can shed light on the different physical conditions and spatial distribution of various elements in the ejecta. Use of such techniques has been commonplace at optical wavelengths, but optically emitting ejecta generally represent a relatively small fraction of the total shocked ejecta mass; few remnants even have significant optical emission from their ejecta to begin with, excepting Cas A and other so-called “oxygen-rich” remnants. The wide bandpass of the ASCA, Chandra, and XMM CCD spectrometers also allows the comparison of relatively hard (4–6 keV) continuum images with softer ( $\lesssim 2$  keV) line images, which has been useful in identifying emission from the forward shock, as discussed below.

Later in this paper, we consider spectral imaging results from Chandra in conjunction with spectroscopic results. Here we consider the recent XMM Newton observation of Tycho's SNR.

## Tycho's SNR with XMM

Tycho's supernova remnant (SN 1572), with its 8' diameter on the sky, is ideally suited for XMM, with its 37' field of view and 6'' PSF core. Tycho's X-ray spectrum is notable for the richness of its line emission, from Fe L transitions (to the n=2 level) with energies near 1 keV, and an exceptionally prominent Si He  $\alpha$  blend near 1.86 keV, to Fe K transitions (to the n=1 level) with energies near 6.4 keV. An imaging study with the ASCA satellite by Hwang & Gotthelf [12] suggested that the Fe L and Fe K emission are not spatially coincident, with the Fe K emission at a smaller average radius than other emission lines. That earlier study is limited by both photon statistics and angular resolution, but new XMM images presented by Decourchelle et al. [13] clearly show that the azimuthally averaged radial distribution of Fe K emission has a peak that lies well inside that of the Fe L emission. By contrast, the Fe L and Si He  $\alpha$  emission are consistent with having the same average radial distribution.

These differences in the radial profiles may be qualitatively understood as arising from the temperature and ionization structure of the ejecta behind the reverse shock. The ejecta of Type Ia supernovae have a steep outer density profile surrounding an inner plateau of more constant density. As the reverse shock reaches the inner plateau in the ejecta distribution, the temperature of the shocked gas should increase and the density decrease. The more recently reverse-shocked gas is therefore hotter and has a lower ionization age, as would be required to explain the presence of Fe K emission at smaller radii, as pointed out by Decourchelle et al. [13]. The low density, hot Fe emission has also been suggested to be associated with radioactively heated bubbles of Fe ejecta by Wang & Chevalier [14]. Detailed further analysis of observations with Chandra and XMM should shed further light on these issues.

## SPATIALLY RESOLVED SPECTROSCOPY

For young remnants whose emission is dominated by their reverse-shocked ejecta, the capability to do detailed spatially resolved X-ray spectroscopy with Chandra and XMM is a wonderful opportunity to study the X-ray emitting ejecta. The XMM observation of Tycho's SNR, for example, straightforwardly confirms the very different compositions of Si and Fe in the two bright knots at the eastern periphery of the remnant [13], a result indicated previously by Vancura et al. [15], but only with considerable data manipulation and luck using the limited instruments then available. XMM isolates the spectra of these knots for the first time. The superior angular resolution of the Chandra mirrors allows one to probe the spectra of even more compact regions, and for this illustration we turn to the brightest Galactic remnant, Cas A.

## Ejecta Knots in Cas A

Cas A has long been considered the undisputed product of the explosion of a massive star, probably a Wolf-Rayet star [16,17], though the compact stellar remnant that then must have been produced remained elusive until Chandra's first light revealed it in X-rays [18–20]. This brief initial observation with the Advanced CCD Imaging Spectrometer (ACIS) also showed that the individual ejecta knots in Cas A have a range of spectral characteristics (Hughes et al. [21]), some of which are qualitatively consistent with their origin in different explosive nucleosynthesis burning zones of a massive star. For instance, the spectrum of a typical knot with emission lines of Si, S, Ar, and Ca was shown to be consistent with the element abundances expected for the zone of explosive O burning, whereas another knot also showing Fe emission is consistent with the zone of incomplete Si burning. A region in the outer southeast region of the remnant that was examined by Hughes et al. required the presence of still more Fe in the ejecta, suggesting a macroscopic mixing and inversion of the Si rich ejecta layer and the innermost layer of Fe.

An observation of Cas A twenty times deeper than the first light observation was also obtained by Chandra. With this observation, the distributions of the Si, S, Ar, Ca, and Fe-emitting ejecta were mapped through the equivalent widths of their emission lines by Hwang, Holt, & Petre [22]. The location of Fe-emitting ejecta mapped in this way is exterior to that of the Si-emitting ejecta throughout the southeast region, but not elsewhere. Because of this singularity of the southeast region, we turn to a more detailed spectral analysis using the deep Chandra observation.

Figure 1 shows the southeastern part of Cas A and indicates the regions studied; the spectral extraction regions were as small as  $3''$  in diameter. The spectra were analyzed using models for plane parallel shocks in XSPEC version 11.0 [23] with a single electron temperature, and including a range of ionization ages from zero up to a fitted maximum value. The ionization age  $n_e t$  is defined as the product of the ambient electron density and the time since the gas was heated by the shock, with equilibrium corresponding to roughly  $10^{12} \text{ cm}^{-3} \text{ s}$  or higher. Also indicated in the figure are the fitted Fe/Si abundance ratios for the various knots, classified broadly as dominated by Si ( $\text{Fe/Si} < 0.1 \text{ Fe}_\odot/\text{Si}_\odot$ ), dominated by Fe ( $\text{Fe/Si} > 1.5 \text{ Fe}_\odot/\text{Si}_\odot$ ) and with a mixture of Fe and Si ( $0.1 \text{ Fe}_\odot/\text{Si}_\odot < \text{Fe/Si} < 1.5 \text{ Fe}_\odot/\text{Si}_\odot$ ). The highest Fe/Si abundance ratios systematically occur in the outermost regions in the southeast, with fitted ratios as high as  $4 - 5 \text{ Fe}_\odot/\text{Si}_\odot$  in the regions that we examined. An intermediate region with a more solar mixture of Si and Fe gives way to a Si-dominated region coincident with the bright ring evident in the broadband images.

Two extreme examples of the spectra for a *single* highly Fe-rich knot and a more typical S-rich knot are shown in Figure 2. Both have a fitted electron temperature of  $kT \sim 2 \text{ keV}$ , that is typical of the ejecta knots. What is obviously very different between the two is the relative abundance of Fe to Si (roughly a factor of 200 higher in the spectrum on the left), that manifests itself in the shape of the continuum

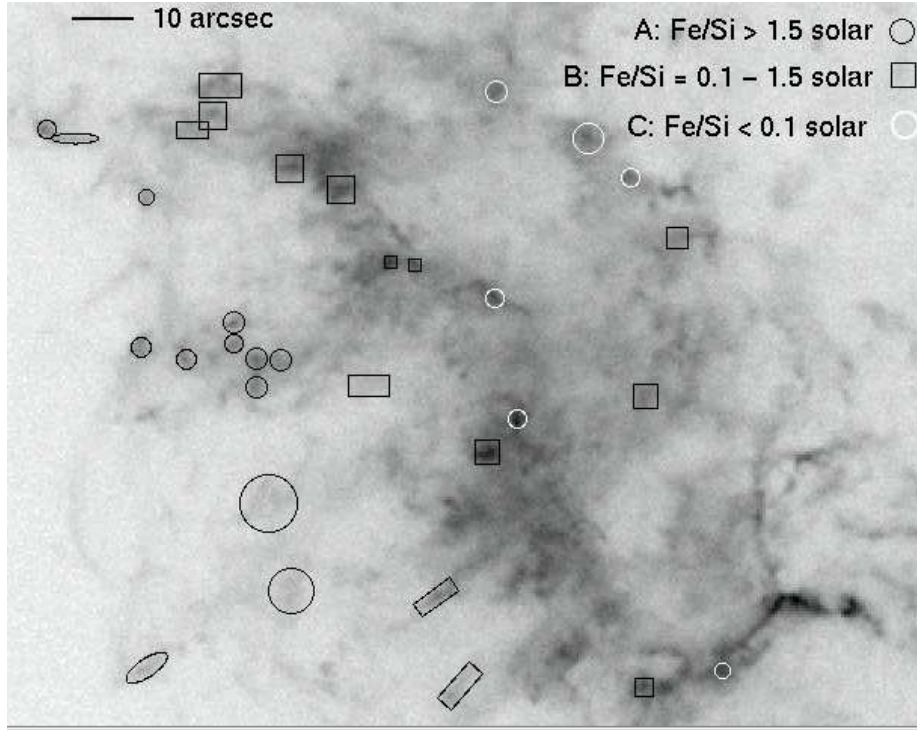


**FIGURE 1.** Closeup view of the southeastern section of Cas A with Chandra ACIS in a deep 50 ks observation (region is  $2.5'$  across). Spectral extraction regions are overlaid and coded according to the fitted Fe/Si element abundance ratio (relative to solar): A (high Fe) circular and elliptical regions, B (mixture) square and rectangular regions, C (high Si) white circular regions.

below the Si blends. Because of the high Fe abundance in the spectrum on the left, this continuum comes predominantly from Fe rather than from H and He. The ionization age  $n_e t$  is also some 50 times higher for the Fe-rich knot than it is for the Si-rich knot. The high ionization age is evident in the shape of the Fe L emission in the spectrum on the left, and is also reflected in the increased strength of the Si Ly  $\alpha$  (2.006 keV) line relative to the Si He  $\alpha$  ( $\sim 1.85$  keV) blend. Assuming that, to zeroth order, the Fe and Si knots were shocked at roughly the same time, this indicates much higher densities in the Fe-rich knots, consistent with their origin deep within the inner layers of the supernova ejecta.

The region of the northeast jet, the largest radial extension seen in Cas A, is well-known from detailed optical observations to be enriched by ejecta emitting in O, S, and Ar [16,17]. The Chandra data show that the X-ray emission arises largely from ejecta highly enriched in Si, Si, Ar, and Ca. Fits to their X-ray spectra also show higher ionization ages than in the bright ring, suggesting that these are also high density clumps flung outward at high velocity during the explosion.

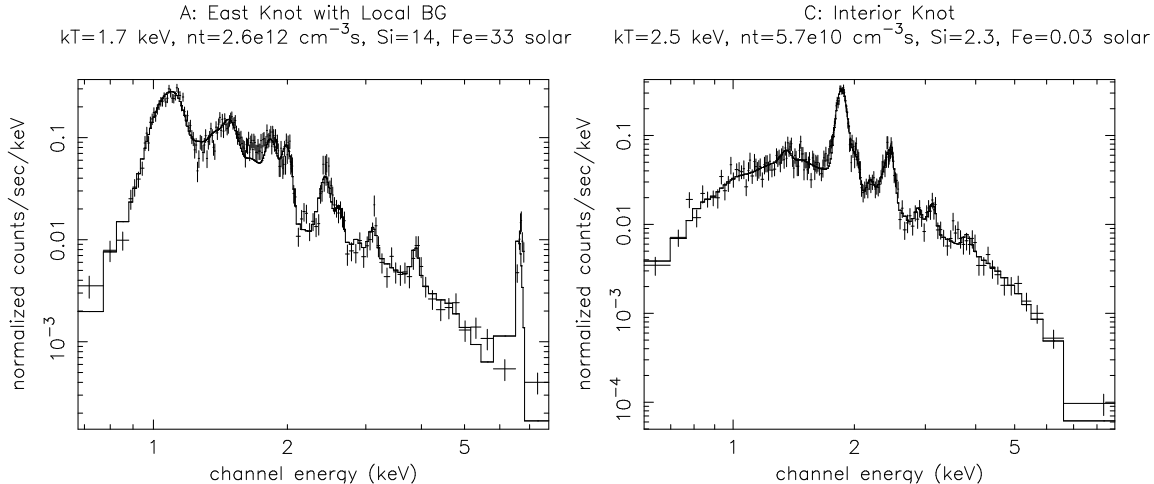


**FIGURE 2.** Representative spectra of extremely Fe- (left) and Si-dominated (right) knots in the southeast region of Cas A. The the best-fit plane-parallel shock model with a single electron temperature is overlaid on the data, and fitted parameter values are indicated.

## ISOLATION OF EMISSION FROM THE FORWARD SHOCK

It was evident from the earliest nonimaging spectral observations that the reverse-shocked ejecta in Tycho and Cas A are the dominant contributors to the soft X-ray emission at energies below about 5 keV [24,1]. The reverse shock cannot exist, however, without the forward shock. For Cas A and Tycho, spatial X-ray components corresponding to the forward shock were suggested from early Einstein observations, for example by Fabian et al. [25] and Seward, Harnden & Tucker [26], and hard components in the spectra were attributed early on to the forward shock (e.g. Pravdo & Smith [27]). The true situation is more complex because theory also predicts nonthermal X-ray emission from particle acceleration at the forward shock and such emission is now observed, with the most famous example being SN1006 [28]. To unambiguously identify the location of the forward shock and to isolate its spectrum, one requires the capability to disentangle spatial and spectral information that is now available with Chandra and XMM.

For Cas A, the Chandra X-ray continuum image at energies between 4 – 6 keV shows a “rim” surrounding the bright ring of emission from the ejecta, as shown by Gotthelf et al. [29]. As discussed elsewhere in these proceedings by Rudnick [30], this is persuasively identified as the location of the forward shock. The location of the forward shock in Tycho is similarly identified by XMM from the good correlation of this X-ray continuum emission with radio emission [13].

At distances of a few kpc within the Galaxy, Cas A and Tycho are relatively nearby, but Chandra’s spatial resolution is good enough to isolate the forward shock in much more distant remnants. The bright ejecta-dominated ring of E0102-72, the

brightest remnant in the Small Magellanic Cloud, has been previously imaged [31] ; Chandra reveals a faint shelf of emission exterior to the ejecta ring that is identified as the forward shock in the observation by Gaetz et al. [32]. The spectrum of this outer region is qualitatively different from that of the ring, as demonstrated by Hughes, Rakowski, & Decourchelle [33], with line strengths that are well-explained by the ambient abundances in the SMC, in contrast to the prominent O and Ne emission from the ejecta-enriched ring. Importantly, the measured temperature of the blast-shocked gas is barely 1 keV. Together with the shock velocity inferred from the measured X-ray expansion of the forward shock, this has the interesting implication that the acceleration of cosmic rays at the forward shock is highly efficient, as the shock should have heated the electrons to substantially higher temperature, even if the electrons equilibrate to the much higher ion temperatures only by Coulomb collisions. It would therefore appear that some of the energy of the shock wave has been diverted elsewhere, with particle acceleration being a persuasive explanation.

## X-RAY DYNAMICAL STUDIES OF REMNANTS

A frontier that will be explored productively, especially by Chandra, is the study of the dynamics of the X-ray emitting gas in remnants. The first X-ray proper motion studies of the youngest and brightest supernova remnants were carried out using the high resolution imaging experiments on the Einstein and ROSAT Observatories, generally for broad radial or azimuthal sectors (Kepler's and Tycho's SNRs by Hughes [34,35], Cas A by Vink et al. [36] and Koralesky et al. [37]). The general trends in these results are two-fold. First, in comparison to similar radio expansion studies [38–41], the X-ray expansion results have yielded velocities that are systematically higher by roughly a factor of two. Second, in spatially resolved expansion studies carried out in both the radio and in X-rays, the expansion is observed to be significantly asymmetric, with expansion rates varying with azimuthal angle by factors of two or even significantly more. Both these points are illustrated in Figure 3 of Rudnick's review of Cas A elsewhere in these proceedings.

The disparity between the radio and X-ray expansion results is disconcerting. In most instances, the extent of the radio and X-ray emission from the remnants is similar, and yet the rate of radio expansion is only about half the rate of the X-ray expansion. Further observations with Chandra over the next several years should help to shed light on this puzzle. In particular, dynamical studies for the brightest remnants could be carried out for individual X-ray knots, and moreover the analysis could be done for each element separately, as has now been done extensively (at least for Cas A and a few other remnants) at optical and radio wavelengths.

The dynamics in the direction along the line of sight can be studied by measuring this velocity component through Doppler shifts in the energies of known emission lines. For Cas A, the presence of asymmetries in the line of sight velocities was known from early observations with the Focal Plane Crystal Spectrometer (FPCS)

on the Einstein Observatory, a dispersive spectrometer that was used in this case with a  $3' \times 30'$  aperture. Markert et al. [42] show that the FPCS spectral scans of He-like Si and S resonance and H-like Ly  $\alpha$  lines from the northwest half of Cas A have lower line energies than those from the southeast, implying bulk motion of the gas in a roughly ring-shaped geometry. A Doppler map by Holt et al. [8] based on the centroid of the Si He  $\alpha$  blend using more recent ASCA data (therefore with lower spectral resolution than the FPCS) confirms and extends this result with an angular resolution of about  $1'$ .

The Chandra version of the Doppler velocity map of Cas A obtained from the centroids of the Si He  $\alpha$  blend is shown in Figure 3. The energy shifts measured correspond to velocities as high as 2500 km/s, with blue-shifted material generally located in the southeast and red-shifted material in the northwest, consistent with previous measurements. The Chandra map gives significantly more detail than previous maps: in the northwest, a concave arc of moderately blueshifted material is seen just south of a convex arc of redshifted material. These structures qualitatively correspond very well with the velocity structure of the dense ejecta knots measured with optical echelle spectra by Lawrence et al. [43], though there is more X-ray emission in the southeast than in the optical. A range of ionization ages is seen in the Si-emitting material in Cas A, and in principle this could affect the centroid of the Si blend, but fortunately the Si energy centroid remains dominated by the resonance line for the relevant range of ionization age and temperature in Cas A. The energy shifts therefore are dominated by Doppler shifts due to the bulk motion of the gas. Even with moderate energy resolution CCD spectrometers, Chandra provides more details of the line-of-sight velocity structure in the X-ray emitting gas than was previously available.

## CONCLUSIONS

Chandra and XMM Newton have opened the way for true spatially resolved X-ray spectroscopy of supernova remnants. Though the CCD spectrometers are limited in their spectral resolution, the ability to disentangle spatial components that change on very small angular scales provides a new window in understanding these complex sources. The results presented in this review are just the beginning!

**Acknowledgements:** It is a pleasure to acknowledge Steve Holt, Rob Petre, and Andy Szymkowiak as my collaborators on the Chandra observation of Cas A, and to thank Anne Decourchelle for generously providing the results of her XMM study of Tycho's supernova remnant prior to publication. We are grateful to Kazik Borkowski for fruitful scientific discussions and for making his spectral models publicly available.

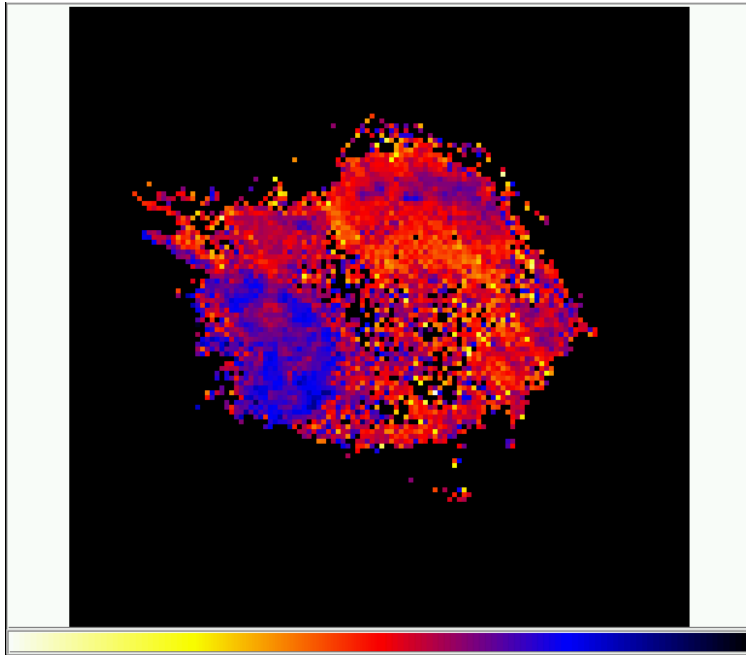


**FIGURE 3.** Doppler velocity map of Cas A based on the Si He  $\alpha$  blend observed with ACIS on Chandra. Black corresponds to blueshifted velocities, white to redshifted velocities. The range of velocity shifts measured is roughly  $\pm 2500$  km/s.

## REFERENCES

1. Becker, R. H., et al. 1979, ApJL, 234, L73
2. Winkler, P. F., Canizares, C. R., Clark, G. W., Markert, T. H., & Petre, R. 1981, ApJ, 245, 574
3. Seward, F. D. 1990, ApJS, 73, 781
4. Aschenbach, B., Egger, R., & Trümper, J. 1995, Nature, 373, 587
5. Levenson, N. A., et al. 1997, ApJ, 484, 304
6. Williams, R. M., et al. 1999, ApJS, 123, 467
7. Tanaka, Y., Inoue, H., & Holt, S. S. 1994, PASJ, 46, L37
8. Holt, S. S., Gotthelf, E. V., Tsunemi, H., & Negoro, H. 1994, PASJ, 46, L151
9. Fujimoto, R., et al. 1995, PASJ, 47, L31
10. Bleeker, J., et al. 2001, A&A, in press
11. Canizares, C. R. 2000, this proceedings
12. Hwang, U., & Gotthelf, E. V. 1997, ApJ, 475, 665
13. Decourchelle, A., et al. 2001, A&A, in press
14. Wang, C.-Y., & Chevalier, R. A. 2000, ApJ, submitted, astro-ph/0005105
15. Vancura, O., Gorenstein, P., & Hughes, J. P. 1995, ApJ, 441, 680
16. Fesen, R. A., Becker, R. H., & Goodrich, R. W. 1988, ApJ, 329, L89
17. Fesen, R. A., & Gunderson, K. S. 1996, ApJ, 470, 967
18. Tananbaum, H., et al. 1999, IAU Circ 7246
19. Pavlov, G., et al. 2000, ApJL, 531, L53

20. Chakrabarty, D., et al. 2000, astro-ph/0001026 preprint
21. Hughes, J. P., Rakowski, C. E., Burrows, D. N., & Slane, P. O. 2000, ApJL, 528, L109
22. Hwang, U., Holt, S. S., & Petre, R. 2000, ApJ, 537, L119
23. Borkowski, K. J., Lyerly, W. J., & Reynolds, S. P. 2000, astro-ph/0008066
24. Becker, R. H., et al. 1980 ApJ, 25, L5
25. Fabian, A. C., et al. 1980, MNRAS, 193, 175
26. Seward, F. D., Gorenstein, P., & Tucker, W. 1983, ApJ, 266, 287
27. Pravdo, S. H., & Smith, B. W. 1979, ApJL, 234, L195
28. Koyama, K., et al. 1995, Nature, 378, 255
29. Gotthelf, E. V., et al. 2000, ApJ, submitted
30. Rudnick, L. 2001, these proceedings
31. Hughes, J. P. 1988, in IAU Colloq. 101, Supernova Remnants and the Interstellar Medium, ed. R. S. Rogers & T. L. Landecker (Cambridge: Cambridge Univ. Press), 125
32. Gaetz, T., et al. 2000, ApJL, 534, 47
33. Hughes, J. P., Rakowski, C. E., & Decourchelle, A. 2000, ApJL, 543, L61
34. Hughes, J. P. 1999, ApJ, 527, 298
35. Hughes, J. P. 2000, ApJ, 545, L53
36. Vink, J., Bloemen, H., Kaastra, J. S., & Bleeker, J. A. M. 1998, A&A, 339, 201
37. Koralesky, B., Rudnick, L., Gotthelf, E. V., & Keohane, J. W. 1998, 505, L27
38. Dickel, J. R., Sault, R., Arendt, R. G., Korista, K. T., & Matsui, Y. 1988, ApJ, 330, 254
39. Reynoso, E. M., Moffett, D. A., Goss, W. M., Dubner, G. M., Dickel, J. R., Reynolds, S. P., & Giacani, E. B. 1997, ApJ, 491, 816
40. Anderson, M. C., & Rudnick, L. 1995, ApJ, 441, 307
41. Agüeros, M. A., & Green, D. A. 1999, MNRAS, 305, 957
42. Markert, T. H., Canizares, C. R., Clark, G. W., & Winkler, P. F. 1983, ApJ, 268, 134
43. Lawrence, S. S., et al. 1995, AJ, 109, 2635